

# Transport in Astrophysics: VII. Solar Modulation of the Cosmic Rays

Lorenzo Zaninetti

Department of Physics, University of Turin, Turin, Italy

Email: l.zaninetti@alice.it

**How to cite this paper:** Zaninetti, L. (2024) Transport in Astrophysics: VII. Solar Modulation of the Cosmic Rays. *International Journal of Astronomy and Astrophysics*, 14, 245-258.

<https://doi.org/10.4236/ijaa.2024.144016>

**Received:** September 4, 2024

**Accepted:** November 2, 2024

**Published:** November 5, 2024

Copyright © 2024 by author(s) and Scientific Research Publishing Inc. This work is licensed under the Creative Commons Attribution International License (CC BY 4.0).

<http://creativecommons.org/licenses/by/4.0/>



Open Access

## Abstract

Two existing solutions for the diffusion of cosmic rays (CRs) are analyzed. The first one is a well-known solution in 3D over an infinite spatial domain and the second one is a 1D solution with an exponential decay initial profile over an infinite spatial domain. For each solution, the temporal evolution of the number of particles at a fixed distance has been analyzed. The anticorrelation between the flux of CRs and the magnetic field at one astronomical unit has been explained by adopting a careful choice of the astrophysical parameters involved.

## Keywords

Cosmic Rays, Particle Diffusion, Random Walks

## 1. Introduction

In order to understand the physics connected with the heliosphere, the monthly mean total sunspot number, which is available starting from 1749, was the first physical phenomenon to be analyzed, see the overall reviews by [1]-[3] or a more localized study of solar cycles 24 - 25 [4]. We now review some recent observations.

1) The electron density, the speed of the solar wind, the radial and total magnetic field and the Alfvén speed were measured as functions of the radial distance from the sun, see [5].

2) The variations in the flux of cosmic rays (CRs) are monitored by a network of ground-based neutron monitors, see [6].

3) The oscillating behavior of the magnetic field at one astronomical unit (au) has been examined by [7].

We now outline some theoretical studies that explain the solar modulation of CRs. The first approach was by Parker in 1958 [8], who correlated the 11-year

variation of the CR intensity with the hydrodynamic outflow of gas from the sun. Numerical solutions for the complete transport equation, which includes the process of adiabatic deceleration together with the processes of diffusion and convection, were considered by [9]. The diffusion tensor based on the theory of turbulence and the theory of charged particle scattering has been analyzed in [10]. The effect of polar perpendicular diffusion and drifts on the propagation of CRs was explored in [11]. The long-term variations of galactic CRs were compared with the behavior of various indices of solar activity and heliospheric parameters during the solar cycle 22 [12]. The influence of spatial and rigidity dependence on the drift coefficient in the modulation of CR carbon in the heliosphere was explored in [13]. The cumulative modulating effect of the interplanetary magnetic field's neutral current sheet and solar activity on propagation of CRs in the heliosphere was analyzed in [14]. The long-term solar modulation of CRs has been modeled by a modified force-field approach [15]. The HELMOD code models the propagation of CRs by solving the Parker transport equation [16]. A global effective formula for the modulation lag of CRs and predictions for the flux evolution of CRs in the solar cycle has been derived by [17]. The stochastically forced solar dynamo model allows long-term simulations that explain how dynamo-generated magnetic fields produce the structure of the heliosphere [18]. The variations of the CRs in the 25th solar cycle were explained by a model based on a forecast of solar activity parameters [19]. Various solutions of the diffusion equation applied to CRs have been explored from a mathematical point of view [20]. Three analytic models were used to explain the solar modulation: the force-field approximation, the convection-diffusion model, and the extended force-field approximation with a drift effect [21]. The above approaches allow posing some questions:

- 1) Can the propagation of CRs be explained by the 1D or 3D time-dependent diffusion in an infinite spatial domain?
- 2) Is it possible to model the anticorrelation between the variable magnetic field of the heliosphere and the concentration of CRs at one astronomical unit?

In order to answer the above questions, Section 2 summarizes the adopted fits and Section 3 reviews the measured data of the heliosphere. Section 4 reviews a well-known 3D solution of the transport equation and a less-known 1D solution. Section 5.1 derives the astrophysical value of the diffusion coefficient. The anticorrelation between the magnetic field and the density of the CRs at one astronomical unit is explained in the framework of 3D diffusion, see Section 5.2, and 1D diffusion, see Section 5.3.

## 2. Adopted Data Analysis

We report the types of fit here used. The oscillatory behavior is modeled by the following sinusoidal fit, which covers many periods:

$$y(t; A, A_0, \omega_0, T) = A \sin\left(\frac{2\pi t}{T} + \omega_0\right) + A_0, \quad (1)$$

where  $A$  is the amplitude of the oscillations,  $A_0$  is the averaged amplitude,  $t$

is the time,  $T$  is the period and  $\omega_0$  is the initial phase.

A fit of gamma type with three parameters is characterized by the following equation, which covers only one period of an oscillatory motion:

$$y(t; a, b, c) = at^b e^{-ct}, \quad (2)$$

where  $a$ ,  $b$  and  $c$  are positive. A power law fit with two parameters is characterized by:

$$y(x; C, \alpha) = Cx^\alpha, \quad (3)$$

where  $x$  is the independent variable,  $C$  is a positive constant and  $\alpha$  is the exponent.

The merit function  $\chi^2$  is given by:

$$\chi^2 = \sum_{i=1}^n \left( \frac{y_i - y_{i,th}}{\sigma_i} \right)^2, \quad (4)$$

where  $n$  is the number of elements of the experimental sample,  $y_{i,th}$  is the theoretical value, and  $\sigma_i$  is the uncertainty in  $y_i$ .

### 3. The Heliosphere

We summarize the observational status of the number of sunspots, the behavior of the magnetic field of the heliosphere, the variations of the flux of the CRs measured by the neutron monitoring stations, and the magnetic field at one au.

#### 3.1. The Number of Sunspots

The monthly mean total number of sunspots for the period 1749-2023 is reported in **Figure 1** as green points.

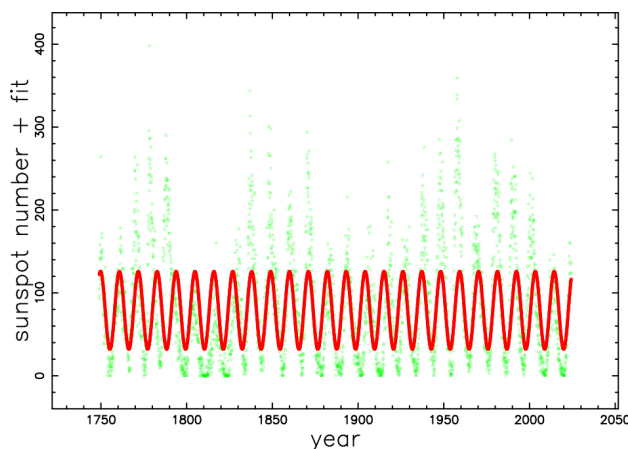


**Figure 1.** Monthly mean total number of sunspots, green points, and sinusoidal fit, red line. The parameters of the sinusoidal fit (1) are  $A = 46.79$ ,  $A_0 = 78.87$ ,  $T = 10.02$  and  $\omega_0 = -2.65$ .

A detailed view of the number of sunspots can be obtained by analyzing solar cycle 24, which started in December 2008, and finished in December 2019, see the

red line in **Figure 2**.

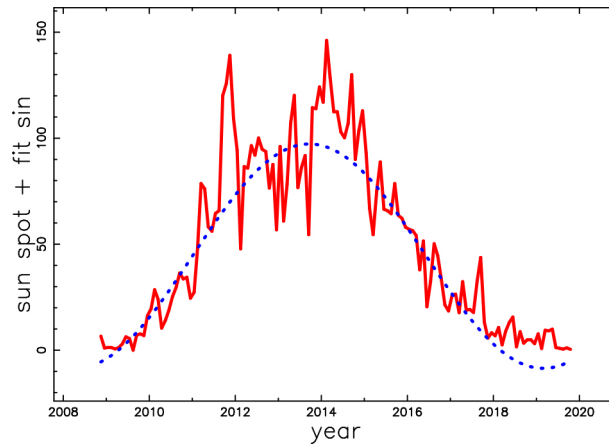


**Figure 2.** Mean total number of sunspots, red line for solar cycle 24, and sinusoidal fit, blue dotted line. The parameters of the fit as represented by Equation (1) are  $A = 52.92$ ,  $A_0 = 44.35$ ,  $T = 10.88$  and  $\omega_0 = -5.15$ . The  $\chi^2$ , according to Formula (4), is 40440.73.

Another type of fit is represented by the three parameters gamma, see the red line in **Figure 3**.

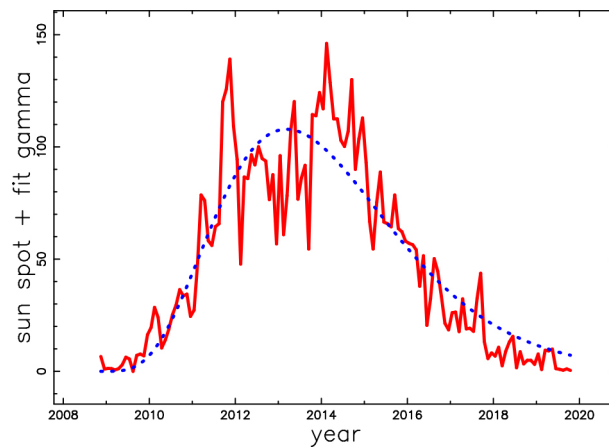


**Figure 3.** Mean total number of sunspots, red line for solar cycle 24, and gamma fit, blue dotted line. The parameters of the gamma fit as represented by Equation (2) are  $a = 13.44$ ,  $b = 4.5$ , and  $c = 1.04$ . The  $\chi^2$ , according to Formula (4), is 39192.

### 3.2. The Magnetic Field of the Heliosphere

The magnetic field of the heliosphere is analyzed in [5] and the data are reported in [22]. That catalog reports the radial magnetic field,  $B_{rad}$ , and the total magnetic field,  $B_{tot}$ . **Table 1** reports minimum, average and maximum of the total component of the magnetic field and **Figure 4** displays its spatial behavior as well as

the power law fit.

**Table 1.** Data of the total magnetic field of the heliosphere in nT.

$B_{min}$	1.732
$\bar{B}$	1233
$B_{max}$	9704

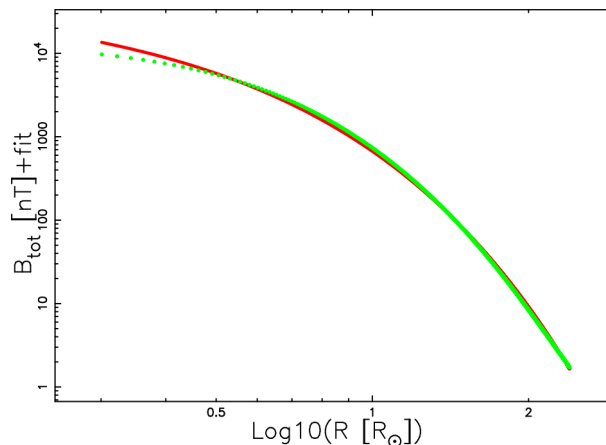


**Figure 4.** The total magnetic field,  $B_{tot}$ , of the heliosphere as function of the distance from the sun in solar radius units, green stars, and fit with a power law are given by Equation (3), red full line. The parameters of the fit are  $C = 49343.7$  and  $\alpha = -1.866$ .

The above power law behavior is transformed to a probability density function (PDF) with the magnetic field expressed in  $\mu$ -gauss units and distance,  $x_{pc}$  in pc:

$$B(x_{pc}) = \frac{2.06 \times 10^{-7}}{x_{pc}^{1.866}} \mu\text{-gauss}. \quad (5)$$

The above PDF allows evaluating the average value of  $x_{pc}$  between the sun and the earth, which is:

$$\bar{x} = \int_{x_l}^{x_u} x_{pc} B(x_{pc}) dx_{pc} = 1.5489 \times 10^{-7} \text{ pc}, \quad (6)$$

where the lower limit,  $x_l$ , corresponds to two  $R_{\odot}$  expressed in pc and the upper limit,  $x_u$ , corresponds to one astronomical unit in pc, which means:

$$\bar{B} = 5207.07 \mu\text{-gauss}. \quad (7)$$

### 3.3. The Neutron Monitoring

The solar modulation is represented by the force-field approximation modeled by the modulation potential  $\Phi$ . In the neutron monitoring stations, the variation of the modulation potential is reported in percent as a function of time, see the red line in **Figure 5**, which is compared with the number of sunspots, see the blue line in **Figure 5**. In **Figure 5**, an anticorrelation is clearly visible between the modulation potential and the sunspots number.

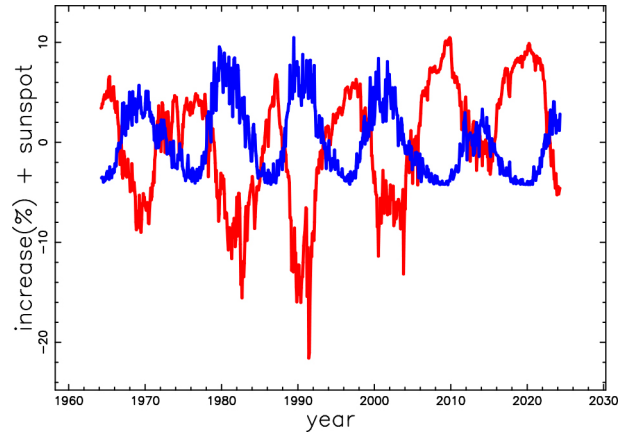


**Figure 5.** Variation of  $\Phi$  in % as function of time and scaled number of sunspots (blue line).

### 3.4. Magnetic Field at 1 au

The interplanetary magnetic field has been modeled by [7] and the variations of the total magnetic field have been recorded at 1 au as a function of time, see **Figure 6**.

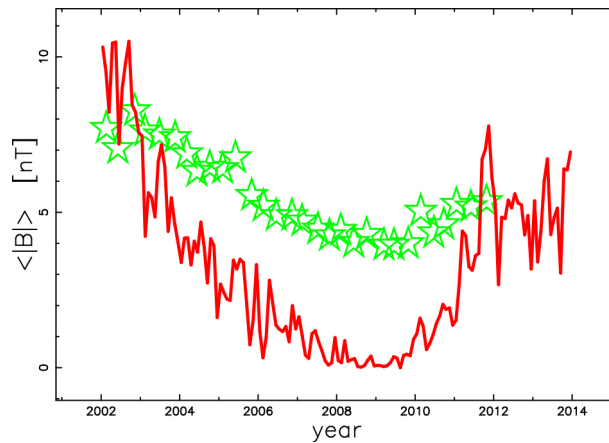


**Figure 6.** Total magnetic field in nT at 1 au (green empty stars) and number of sunspots (red line).

In the above figure, a correlation between the total magnetic field at 1 au and the number of sunspots is clearly visible.

## 4. Diffusion

Many approaches to the diffusion coefficient for CRs,  $D$ , are based on the following definition:

$$D = K(E) \sim E^\delta, \quad (8)$$

with  $\delta \approx 0.3 - 0.6$  [23]. Here, conversely, we adopt a diffusion coefficient based on the relativistic free path and the transport velocity. The time-dependent diffusion equation for CRs is here analyzed in its simplest form: a well-known 3D

impulsive solution of the diffusion equation in an infinite domain and a less-known 1D solution of the diffusion equation with an existing profile in an infinite domain.

#### 4.1. The Diffusion Coefficient

The dependence for the mean square displacement of the random walk,  $\overline{R^2(t)}$ , according to Equation (8.38) in [24], is:

$$\overline{R^2(t)} = 2dDt \quad (t \rightarrow \infty), \quad (9)$$

where  $d$  is the number of spatial dimensions. From Equation (9), the diffusion coefficient is derived in the continuum:

$$D = (t \rightarrow \infty) \frac{\overline{R^2}}{2dt}. \quad (10)$$

Using discrete time steps, the average square radius after  $N$  steps, Equation (12.5) in [24], is:

$$\langle R^2(N) \rangle \sim 2dDN, \quad (11)$$

from which the diffusion coefficient is derived:

$$D = \frac{\langle R^2(N) \rangle}{2dN}. \quad (12)$$

If  $\langle R^2(N) \rangle \sim N$ , the diffusion coefficient is:

$$D = \frac{1}{2d} \lambda v_{tr}, \quad (13)$$

when the step length of the walker or mean free path between successive collisions is  $\lambda$  and the transport velocity is  $v_{tr}$ .

#### 4.2. 3D Case, Impulsive Injection

In 3D, Fick's second law in spherical coordinates is:

$$D \left( \frac{2 \left( \frac{\partial}{\partial r} N(r,t) \right)}{r} + \frac{\partial^2}{\partial r^2} N(r,t) \right) = \frac{\partial}{\partial t} N(r,t), \quad (14)$$

which has a solution:

$$N(r,t;D) = \frac{N_0 \sqrt{4e^{-\frac{r^2}{4Dt}}}}{16(\pi Dt)^{\frac{3}{2}}}, \quad (15)$$

where  $N_0$  is the number of particles injected at  $t=0$  and  $r=0$ . Once the radius of the sphere,  $r$  is fixed, the maximum number of particles occurs at time:

$$t_{max} = \frac{r^2}{6D}. \tag{16}$$

A display of the concentration of particles at fixed distance and variable time in 3D is presented in **Figure 7** for two values of the diffusion coefficient. The maximum concentration for this 3D solution is clearly dependent on the value of the diffusion coefficient.

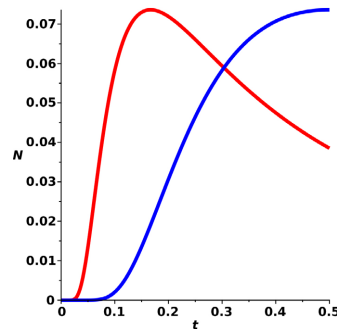


**Figure 7.** Number of diffusing particles in 3D when  $N_0=1$  and  $r=1$ :  $D=1$  red line and  $D=1/3$  blue line.

### 4.3. 1D Case with an Existing Profile

We analyze the case of 1D diffusion in an infinite domain with an initial exponential profile. The equation for the diffusion is:

$$\dot{u}(x,t) = D \left( \frac{\partial^2}{\partial x^2} u(x,t) \right), \tag{17}$$

where  $D$  is the diffusion coefficient and  $u(x,t)$  is the concentration of particles. The initial condition is  $u(x,0) = f(x)$  with:

$$f(x) = N_0 e^{-\frac{x^2}{b^2}}, \tag{18}$$

where  $N_0$  is the maximum concentration and  $b$  is the scale of the existing concentration. The solution is:

$$u(x,t) = \frac{bN_0 e^{-\frac{x^2}{4Dt+b^2}}}{\sqrt{4Dt+b^2}}. \tag{19}$$

Once the distance on the line,  $x$  is fixed, and  $x > \frac{\sqrt{2}b}{2}$ , the maximum number of particles occurs at time:

$$t_{max} = -\frac{b^2 - 2x^2}{4D}. \tag{20}$$

A display of the typical maximum in concentration as a function of time is presented in **Figure 8**. Also, for this 1D solution, the maximum concentration is dependent on the value of the diffusion coefficient.

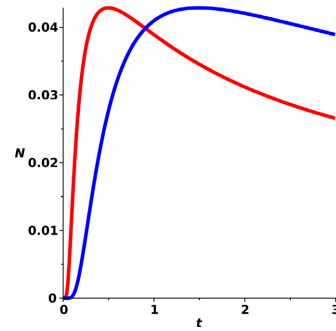


**Figure 8.** Number of diffusing particles in 1D when  $N_0=1$  and  $x=1$ :  $D=1$  red line and  $D=1/3$  blue line.

## 5. Astrophysical Applications

Is important to stress that in the following we will have two times, one astronomical of the order of 11 years,  $t_{\text{astro}}$ , and the other one characteristic of the diffusion,  $t_{\text{diff}}$ , less that 1/10 of a year. We now report the astrophysical value of the diffusion coefficient, a 3D impulsive simulation and a 1D simulation with an initial profile.

### 5.1. The Astrophysical Diffusion Coefficient

The relativistic gyroradius or Larmor radius of a single CR is:

$$r_H = \frac{mc\gamma v_{\perp}}{qB}, \quad (21)$$

where  $m$  is the mass of the particle,  $c$  is the speed of light,

$$\gamma = \frac{1}{\sqrt{1 - \frac{v^2}{c^2}}}, \quad (22)$$

is the Lorentz factor,  $v$  is the velocity of the particle,  $q$  is the charge of the ,  $B$  is the magnetic field and  $v_{\perp}$  is the velocity of the particle perpendicular to the magnetic field, as seen in Formula (1.54) in [25] or Formula (7.3) in [26]. We now assume  $v_{\perp} = c$  due to the fact that we are dealing with relativistic particles. The numerical value of the Larmor radius in the case of an accelerator is, in SI units,

$$r_L \approx \frac{3.335 E_{\text{GeV}}}{B_T} \text{m}, \quad (23)$$

where  $E_{\text{GeV}}$  is the energy expressed in GeV and  $B_T$  is the magnetic field expressed in tesla. In the case of a CR, we express the Larmor radius in pc:

$$r_L \approx \frac{1.081 E_{\text{PeV}}}{Z B_{-6}} \text{pc}, \quad (24)$$

where  $Z$  is the atomic number,  $E_{\text{PeV}}$  is the energy expressed in  $10^{15}$  eV, and  $B_{-6}$  is the magnetic field expressed in  $10^{-6}$  gauss, see [27]. On assuming that the CRs diffuse with a mean free path equal to the relativistic gyroradius, the transport

velocity is equal to the speed of light and  $d = 3$ , the diffusion coefficient according to Equation (13) is:

$$D = \frac{0.055134 E_{peV} \text{ pc}^2}{Z B_{-6} \text{ year}} = \frac{5.5134 \times 10^{-8} E_{GeV} \text{ pc}^2}{Z B_{-6} \text{ year}}. \tag{25}$$

The difference with the diffusion coefficient as given by Equation (8) is that here we have a linear dependence on the energy against a power law, further on the constant  $K$  of Equation (8) is numerically evaluated on the basis of the physics involved. As an example when  $E_{peV} = 10^{-5}$ ,  $Z = 1$ ,  $B_{-6} = 5207.07$  and  $d = 3$  we have  $D = 1.0588 \times 10^{-10} \text{ pc}^2 \cdot \text{year}$ . In order to evaluate the diffusion time from the sun to earth (1 au), we insert in Equation (9) the above value of the diffusion coefficient and we choose  $\sqrt{R^2(t)} = 1 \text{ au} = 4.84814 \times 10^{-6} \text{ pc}$ , obtaining  $t_{diff} = 0.03699 \text{ year}$ .

### 5.2. Simulation with a 3D Impulse

We now outline how it is possible to have an anticorrelation between the magnetic field and the number of diffusing CRs. We assume that the average magnetic field between the sun and the earth oscillates with the following law:

$$B_6(t) = A + A/10 \sin\left(\frac{2\pi t_{astro}}{T}\right), \tag{26}$$

where  $A = 5207.07 \text{ } \mu\text{-gauss}$  is the average magnetic field between the sun and the earth, see Equation (7),  $t_{astro}$  is the astronomical time and  $T = 12 \text{ yr}$ . The difference between the number of diffusing particles at the maximum average magnetic field and that at the average magnetic field is shown in **Figure 9**.

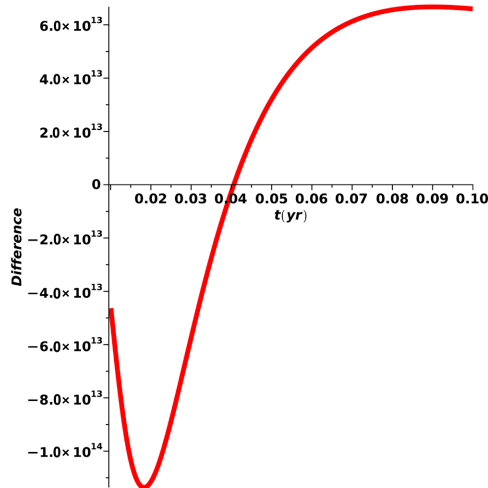


**Figure 9.** Difference between number of diffusing particles at  $B = 1.2 \times 5207.07 \text{ } \mu\text{-gauss}$  and  $B = 5207.07 \text{ } \mu\text{-gauss}$  when  $E_{peV} = 10^{-5}$ ,  $Z = 1$ , and  $d = 3$ .

This means there is an anticorrelation between the oscillating averaged magnetic field and the concentration of CRs, see **Figure 10**.

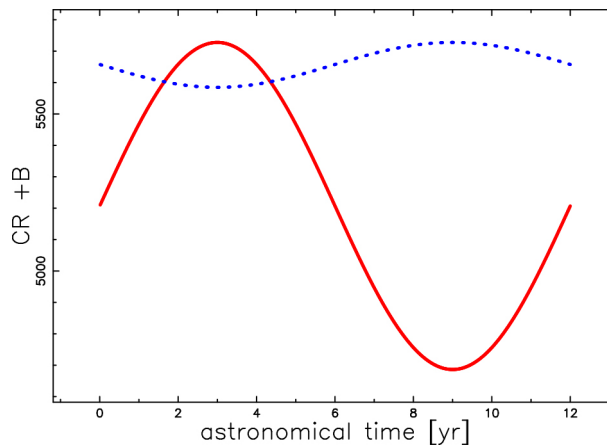


**Figure 10.** Oscillating average magnetic field (blue dots) and superposed behavior for the 3D concentration of CR (red line) when  $E_{PeV} = 10^{-5}$ ,  $Z = 1$ ,  $t_{burst} = 0.01$  yr,  $T = 12$  yr and  $d = 3$ .

The above bursting time,  $t_{burst} = 0.01$  yr = 19423.73 min, can be compared with the time necessary to travel from the sun to 1 au,  $t_{light} = 0.00001584308739$  yr = 8.3176208 min, which means in the framework of the 3D random walk 2335 collisions, see Equation (12).

### 5.3. Simulation with a 1D Profile

The average magnetic field between the sun and the earth is assumed to oscillate according to Equation (26). The number of dimensions is now 1,  $d = 1$ , and the diffusion coefficient according to Equation (13) is:

$$D = \frac{0.1654 E_{PeV} \text{ pc}^2}{Z B_{-6} \text{ year}}. \quad (27)$$

The concentration of CRs in 1D is shown in **Figure 11** in which the anticorrelation with the oscillating averaged magnetic field is clearly outlined.

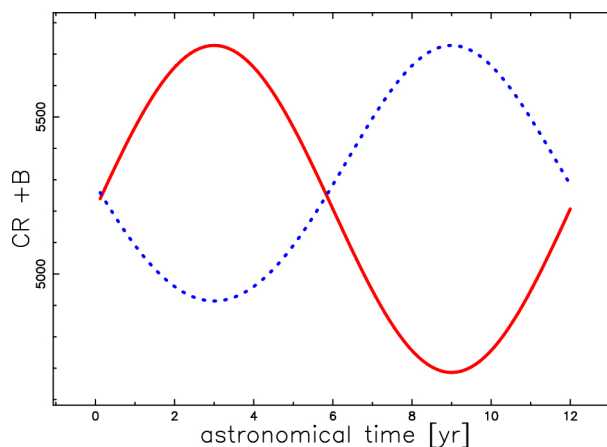


**Figure 11.** Oscillating average magnetic field (blue dots) and superposed behavior for the 1D concentration of CR (red line) when  $E_{PeV} = 10^{-5}$ ,  $Z = 1$ ,  $t_{burst} = 0.01$  yr,  $T = 12$  yr and  $d = 1$ .

## 6. Conclusions

### 6.1. PDE

Two solutions of the diffusion equation over an infinite domain have been reviewed: the first one, which is well known, covers the case of the 3D diffusion in the presence of an initial impulse of particles, see Equation (15); the second one gives the 1D diffusion for the case of an exponential profile for the number of particles, see Equation (19). Particular attention has been paid in both cases to the maximum concentration as a function of time when the distance is fixed, see Formulae (20) and (16) or **Figure 10** and **Figure 11**. In future work, we plan to make a comparison between different solutions of the diffusion equation of CRs in the framework of the heliosphere's physical parameters.

### 6.2. Anticorrelation

The anticorrelation between the magnetic field at one au and the concentration of CRs is explained by a careful choice of the parameters that characterize the diffusion, in particular, the oscillating behavior of the average magnetic field and the superposed behavior for the 3D concentration of CRs are shown in **Figure 10**. **Figure 11** shows the oscillating behavior of the average magnetic field and the superposed behavior for the 1D concentration of CRs.

## Acknowledgments

The data on the number of sunspots are courtesy of the WDC-SILSO, Royal Observatory of Belgium, Brussels and are available at <https://www.sidc.be/SILSO/home>, in particular, the file: monthly mean total sunspot number [1/1749 - now]. We acknowledge the Neutron Monitor Database, NMDB, available at <http://www01.nmdb.eu/next/search.php>, in particular, we selected the period 1964-2024 of the Oulu station. The values of the interplanetary magnetic field have been extracted by the author from Figure 2 of [7].

## Conflicts of Interest

The author declares no conflicts of interest regarding the publication of this paper.

## References

- [1] Solanki, S.K. (2003) Sunspots: An overview. *Astronomy and Astrophysics Review*, **11**, 153-286. <https://doi.org/10.1007/s00159-003-0018-4>
- [2] Vaquero, J.M. (2007) Historical Sunspot Observations: A Review. *Advances in Space Research*, **40**, 929-941. <https://doi.org/10.1016/j.asr.2007.01.087>
- [3] Hayakawa, H., Hattori, K., Sôma, M., Iju, T., Besser, B.P. and Kosaka, S. (2022) An Overview of Sunspot Observations in 1727-1748. *The Astrophysical Journal*, **941**, Article No. 151. <https://doi.org/10.3847/1538-4357/ac6671>
- [4] Nandy, D. (2021) Progress in Solar Cycle Predictions: Sunspot Cycles 24-25 in Perspective. *Solar Physics*, **296**, Article No. 54. <https://doi.org/10.1007/s11207-021-01797-2>

- [5] Mann, G., Warmuth, A., Vocks, C. and Rouillard, A.P. (2023) A Heliospheric Density and Magnetic Field Model. *Astronomy & Astrophysics*, **679**, A64. <https://doi.org/10.1051/0004-6361/202245050>
- [6] Väisänen, P., Usoskin, I., Kähkönen, R., Koldobskiy, S. and Mursula, K. (2023) Revised Reconstruction of the Heliospheric Modulation Potential for 1964-2022. *Journal of Geophysical Research: Space Physics*, **128**, e2023JA031352. <https://doi.org/10.1029/2023ja031352>
- [7] Smith, C.W., Schwadron, N.A. and DeForest, C.E. (2013) Decline and Recovery of the Interplanetary Magnetic Field During the Protracted Solar Minimum. *The Astrophysical Journal*, **775**, Article No. 59. <https://doi.org/10.1088/0004-637x/775/1/59>
- [8] Parker, E.N. (1958) Cosmic-Ray Modulation by Solar Wind. *Physical Review*, **110**, 1445-1449. <https://doi.org/10.1103/physrev.110.1445>
- [9] Lezniak, J.A. and Webber, W.R. (1971) Solar Modulation of Cosmic Ray Protons, Helium Nuclei, and Electrons: A Comparison of Experiment with Theory. *Journal of Geophysical Research*, **76**, 1605-1624. <https://doi.org/10.1029/ja076i007p01605>
- [10] Parhi, S., Bieber, J.W., Matthaeus, W.H. and Burger, R.A. (2003) Toward an *Ab Initio* Theory of the Solar Modulation of Cosmic Rays. *The Astrophysical Journal*, **585**, 502-515. <https://doi.org/10.1086/345988>
- [11] Potgieter, M.S. and Langner, U.W. (2005) Modulation of Cosmic Rays: Perpendicular Diffusion and Drifts in a Heliosphere with a Solar Wind Termination Shock. *Advances in Space Research*, **35**, 554-561. <https://doi.org/10.1016/j.asr.2005.01.008>
- [12] Mavromichalaki, H., Paouris, E. and Karalidi, T. (2007) Cosmic-Ray Modulation: An Empirical Relation with Solar and Heliospheric Parameters. *Solar Physics*, **245**, 369-390. <https://doi.org/10.1007/s11207-007-9043-1>
- [13] Ngobeni, M.D. and Potgieter, M.S. (2015) Modelling the Effects of Scattering Parameters on Particle-Drift in the Solar Modulation of Galactic Cosmic Rays. *Advances in Space Research*, **56**, 1525-1537. <https://doi.org/10.1016/j.asr.2015.06.034>
- [14] Gololobov, P., Krivoshapkin, P., Krymsky, G. and Gerasimova, S. (2020) Investigating the Influence of Geometry of the Heliospheric Neutral Current Sheet and Solar Activity on Modulation of Galactic Cosmic Rays with a Method of Main Components. *Solar-Terrestrial Physics*, **6**, 24-28. <https://doi.org/10.12737/stp-61202002>
- [15] Shen, Z., Yang, H., Zuo, P., Qin, G., Wei, F., Xu, X., *et al.* (2021) Solar Modulation of Galactic Cosmic-Ray Protons Based on a Modified Force-Field Approach. *The Astrophysical Journal*, **921**, Article No. 109. <https://doi.org/10.3847/1538-4357/ac1fe8>
- [16] Boschini, M.J., Della Torre, S., Gervasi, M., La Vacca, G. and Rancoita, P.G. (2022) The Transport of Galactic Cosmic Rays in Heliosphere: The Helmod Model Compared with Other Commonly Employed Solar Modulation Models. *Advances in Space Research*, **70**, 2636-2648. <https://doi.org/10.1016/j.asr.2022.03.026>
- [17] Tomassetti, N., Bertucci, B. and Fiandrini, E. (2022) Temporal Evolution and Rigidity Dependence of the Solar Modulation Lag of Galactic Cosmic Rays. *Physical Review D*, **106**, Article ID: 103022. <https://doi.org/10.1103/physrevd.106.103022>
- [18] Dash, S., Nandy, D. and Usoskin, I. (2023) Long-Term Forcing of the Sun's Coronal Field, Open Flux, and Cosmic Ray Modulation Potential during Grand Minima, Maxima, and Regular Activity Phases by the Solar Dynamo Mechanism. *Monthly Notices of the Royal Astronomical Society*, **525**, 4801-4814. <https://doi.org/10.1093/mnras/stad1807>
- [19] Yanke, V.G., Belov, A.V., Gushchina, R.T., Kobelev, P.G. and Trefilova, L.A. (2024) Forecast of Modulation of Cosmic Rays with Rigidity of 10 GV in the 25th Solar Activity Cycle. *Geomagnetism and Aeronomy*, **64**, 201-210.

- <https://doi.org/10.1134/s0016793223601072>
- [20] Raghavendra, R. and Annareddy, S.K. (2024) Cosmic Ray Diffusion and Evolution: 1d, 2d, and 3d Insights. *Journal of Theoretical Physics & Mathematics Research*, **2**, 1-16.
- [21] Long, W. and Wu, J. (2024) Probing Solar Modulation Analytic Models with Cosmic Ray Periodic Spectra. *Physical Review D*, **109**, Article ID: 083009. <https://doi.org/10.1103/physrevd.109.083009>
- [22] Mann, G., Warmuth, A., Vocks, C. and Rouillard, A.P. (2023) A Heliospheric Density and Magnetic Field Model. *Astronomy & Astrophysics*, **679**, A64. <https://doi.org/10.1051/0004-6361/202245050>
- [23] Tomassetti, N. (2023) Direct Measurements of Galactic Cosmic Rays. *Proceedings of 27th European Cosmic Ray Symposium—PoS (ECRS)*, Nijmegen, 25-29 July 2022, 1-21. <https://doi.org/10.22323/1.423.0007>
- [24] Gould, H. and Tobochnik, J. (1988) An Introduction to Computer Simulation Methods. Addison-Wesley.
- [25] Lang, K.R. (1999) Astrophysical Formulae. Third Edition, Springer.
- [26] Longair, M.S. (2011) High Energy Astrophysics. 3rd Edition, Cambridge University Press. <https://doi.org/10.1017/cbo9780511778346>
- [27] Hillas, A. (1984) The Origin of Ultra-High-Energy Cosmic Rays. *Annual Review of Astronomy and Astrophysics*, **22**, 425-444. <https://doi.org/10.1146/annurev.astro.22.1.425>